Low-Temperature Solution-Processed Thin SnO₂/Al₂O₃ Double Electron Transport Layers Towards 20% Efficient Perovskite Solar Cells

Janardan Dagar,[a] Sergio Castro-Hermosa[a], Giulia Lucarelli[a, b], Andrea Zampetti[b], Franco Cacialli[b],

Thomas M. Brown[a,*]

Abstract— We present planar perovskite solar cells (PSCs) incorporating thin SnO₂/Al₂O₃ double electron transport layers between the perovskite and an indium tin oxide (ITO) bottom electrode. When measured under 1 sun illumination, we obtained a maximum power conversion efficiency (PCE) of 20.1% and a steady state efficiency of 17.8% for the best cell. These values were ~ 20-30% higher in relative terms than that of cells with SnO₂ only (i.e. a maximum PCE of 15.3% and a steady state PCE of 14.9%). Insertion of the thin UV-irradiated solution-processed nanoparticle Al₂O₃ interlayer effectively enhanced the wettability of the electron transport layer, provided enhanced interface area, as well as a lower work function, leading to improved charge extraction. Incorporation of an Al₂O₃ layer between the perovskite and SnO₂ layers also improved the rectification ratios of the diodes as well as both series and shunt resistances. Our devices are fabricated using fully solution-processed transport and active semiconducting layers processed at low temperatures (≤ 150 °C).

Index Terms— electron transport layer, maximum power point tracking, SnO₂ layer, SnO₂/Al₂O₃ double layer, planar perovskite solar cell.

I. INTRODUCTION

Organic–inorganic hybrid perovskite solar cells (PSCs) have attracted tremendous attention due to their high power conversion efficiency (PCE), and low-cost fabrication processes [1-7]. The highest efficiency of the PSCs reported so far is 24.2% [8]. In order to achieve high efficiencies, great care has been put into material processing, device processing, architectures and interfaces [9, 10]. Generally, PSCs are composed of p-i-n or n−i−p configurations where the photo-absorbing perovskite layer is incorporated between a hole transport layer (HTL) and an electron transport layer (ETL). These transport layers extract photo-generated electrons and holes from the perovskite towards the electrodes. To date, several electron transport layers (ETLs) have been developed in the popular n-i-p configuration, including SnO₂ [10, 11], ZnO [12-14], TiO₂, [15]. "Notably, fullerenes have also been used as effective ETLs in both n-i-n and p-i-n perovskite solar cells configurations due to a number of capabilities including passivating surface defects and filtering the UV light reaching the photoabsorbing layer. Fullerene-based ETLs not only improve the performance of the PSCs but also reduce the hysteresis during the JV scans in forwards and reverse directions [16, 17]. TiO₂ has historically been the most

common ETL used in n-i-p PSCs which is typically annealed at high temperature (>450 °C), in a process that is flexible and also adaptable to 3D nanostructuring via a variety of approaches, including nanosphere templating to aid photon recycling [18]. Here, we used a SnO_2 ETL due to its potential properties including high optical transparency, and the wider band gap compared to TiO_2 ETL [19-21]. The SnO_2 ETL is processed at low temperature (≤ 150 °C) along with UV light treatment. However, the performance of PSCs utilizing "low-temperature" SnO_2 deposited from $SnCl_2.2H_2O$ precursor solution dissolved in hydrous ethanol (0.1M concentration) is not always at the same level as that obtained from "high-temperature alternatives", and show less reproducibility and significant hysteresis due to the presence of surface traps at the interface of SnO_2 and perovskite layer. Several treatments to the SnO_2 layer including UV light exposure [11], water vapor treatments [22], together with plasma-enhanced atomic-layer deposition (PEALD) [23] have been carried out in order to enhance the performance of SnO_2 based PSCs. Another route consists in developing composite ETLs. Recently, we have shown that applying a thin MgO (magnesium oxide) coating over the SnO_2 delivered a ~ 20% increase in PCE compared to devices with SnO_2 only ETLs [4]. Here, we introduce a different oxide nanolayer, made of Al_2O_3 nanoparticles (NPs) with average size of <50 nm, rather than the customary thicker mesoporous TiO_2 or Al_2O_3 scaffolds typically used in PSCs [24-26], over the SnO_2 reaching an enhancement of 20-30% in PCE compared to cells with SnO_2 only, utilizing exclusively low-temperature fabrication procedures (i.e. below 150 °C) and the most simple of perovskite active layers, i.e. $CH_3NH_3PbI_3$.

II. EXPERIMENTAL

A. Materials

Al_2O_3 (Aluminum oxide) nanopowder, <50 nm particle size, Tin chloride ($SnCl_2.2H_2O$) dehydrate, 4-tert-butylpyridine (TBP), Li-bis(trifluoromethanesulfonyl) imide (Li-TFSI) and solvents DMSO (Dimethyl sulfoxide anhydrous, $\geq$99.9%), DMF (*N,N*-Dimethylformamide anhydrous, 99.8%), ethanol (99.8%), diethyl ether (99.0%) were purchased from Sigma-Aldrich. Lead(II) Iodide (99.99%, trace metals basis) was purchased from TCI Deutschland gmbh. Methylammonium iodide (CH_3NH_3I) and FK209 cobalt salt (98%) were purchased from Dyesol Limited. 2,2',7,7'-tetrakis-(N,N-di-p-methoxyphenylamine)-9,9'-spirobifluorene (spiro-meotad) ($\geq$99.8%) was purchased from Borum New Material technology Ltd.

B. Device Fabrication

Glass/ITO substrates (Kintec -8Ω/$\square$, 25x25 mm) were realized over specific layout of the ITO electrode using a raster scanning laser (Nd:YVO4, $\lambda = 1064$ nm, 8 ns, pulsed at 10 kHz with a fluence of 260 mJ/cm²) [27]. The patterned ITO substrates were cleaned in ultrasonic bath using acetone, and isopropanol for 15 minutes each, followed by drying with compressed air. The substrates were transferred under a UV-lamp with an estimated power density of 225 mW cm^{-2} (Dymax EC 5000 UV lamp with a metal-halide bulb PN38560 Dymax that contains no UV-C) for 10 minutes. The UV-light treatment over glass/ITO surface assist the removal of organic residues and lead to enhance the wettability of ITO cathode. For the fabrication of ITO/SnO_2/Al2O3/$CH_3NH_3PbI_3$/Spiro-MeOTAD/Au perovskite solar cell devices, SnO_2 solution, 0.1M in ethanol from $SnCl_2.2H_2O$ precursor bought from sigma Aldrich [28] was spin coated over Glass/ITO substrates at 1500 rpm for 30 second and followed by 2500 rpm for next 30 second for obtaining a thickness of 24-30 nm, which was confirmed by profilometer. The substrates were annealed on a hotplate at 150 °C in ambient air for 1 hour, followed by a UV-light irradiation treatment for 15 minutes.

The Al_2O_3 solution was prepared by diluting Al_2O_3 dispersion (Al_2O_3 nanoparticles, <50 nm particle size (DLS), 20 wt. % in isopropanol) in isopropanol (1.78 mg/ml) followed by overnight stirring at room temperature. The Al_2O_3 layer was spin coated over the SnO_2 layer at 1000, 3000, 5000 and 6000 rpms for 30 seconds for each concentration. The substrates with Al_2O_3 layer were annealed at 150 °C for 1 hour in air and further subjected to a UV light irradiation treatment for 15 minutes. The perovskite films were deposited by the so-called single-step solvent-engineering method[29]. The perovskite solution was prepared by dissolving mixture of 1.41 M of PbI_2 and 1.41 M CH_3NH_3I in DMF: DMSO 9:1 (v/v) solvents and overnight stirring at room temperature.

The perovskite solution was deposited over ETLs layer via spin coating at spin speeds of 1000 rpms for 10 seconds and then 5000 rpms for 45 sec. Next, 0.7 mL of diethyl ether were dropped on the rotating substrates when 35 seconds are remaining. Further to obtain a homogeneous and mirror-like black perovskite film these were successively subjected to a two-step annealing process, carried out at 50 °C for 2 minutes and then at 100 °C for 10 minutes [4, 28, 30, 31] .

As a hole transport layer, Spiro-OMeTAD solution in chlorobenzene (74 mg·mL^{-1}) was deposited via spin coating at spin speed of 2000 rpm for 20 under inert atmosphere. The solution was doped with LiTFSI (16.6µL/mL), TBP (26.77µL/mL), and cobalt(III) complex (7.2 µL/mL) and kept overnight at room temperature in inert atmosphere [30]. Finally, the samples were inserted in to high vacuum chamber (10^{-6} mbar) to evaporate gold (Au) as back contacts (thickness~80nm) through a shadow mask.

C. Device measurements

The perovskite solar cells were tested under a AM1.5G Class A ABET solar simulator at an intensity of 1000 W/m² (1 sun) illumination conditions, calibrated with a EKO MS-602 pyranometer. Current-voltage characteristics were obtained using a digital source meter (Keithley 2420) [37]. The LabVIEW parameters including voltage step and delay time

for data point scans were fixed at 30 mV and 200 ms respectively during the measurements. Solar cells were

minute, or k rpm) in order to investigate which processing parameters were optimal for device performance [35].

Al$_2$O$_3$ conc.(mg/ml)	Electron Transport Layer	Al$_2$O$_3$ Spin Speed (rpm)	J$_{sc}$ [mA/cm^2]	V$_{oc}$ [V]	FF [%]	PCE [%]	PCE Max[%]
None	SnO$_2$	No	20.08 ± 0.68	1.08 ± 0.02	66.80 ± 1.43	14.58 ± 1.07	15.3
1.78	SnO$_2$/Al$_2$O$_3$	1000	21.53 ± 0.60	1.13 ± 0.005	72.34 ± 2.00	17.61 ± 0.66	18.6
	SnO$_2$/Al$_2$O$_3$	3000	22.87 ± 1.22	1.14 ± 0.011	73.14 ± 1.96	19.10 ± 0.97	20.1
	SnO$_2$/Al$_2$O$_3$	5000	20.92 ± 0.41	1.12 ± 0.004	75.15 ± 1.83	17.73 ± 0.84	18.4
	SnO$_2$/Al$_2$O$_3$	6000	20.75 ± 0.68	1.12 ± 0.005	72.77 ± 2.02	16.94 ± 0.12	17.1

measured with an aperture of 0.1 cm^2 using a black tape mask and fixed in a Teflon holder to keep them flat under sun light illumination. The average PV parameters, shown in the main text were measured in reverse scan. Forward scans are also reported for the best cells as well as the steady state power conversion efficiency [4, 26, 32].

The EQE (external quantum efficiency) measurements of perovskite solar cells were carried out using a homemade apparatus consisting of an amperometer (Keithley 2612) and a monochromator (Newport 74000).

The dark J-V characteristics and open circuit voltage rise/decay measurements were carried out using a modular testing platform (Arkeo - Cicci research s.r.l.). The Arkeo system refers to a white LED array (4200 K) which can be tuned up to 200 mW/cm^2 of optical power intensity and high speed source meter unit [33] [39].

Here we focus only on the formulation that delivered the best-performing solar cells, i.e. those from the 1.78mg/ml Al$_2$O$_3$ solution. The current density-voltage (J-V) characteristics of the best performing PSCs with Al$_2$O$_3$ interlayers deposited at different spin speeds measured under 1 sun illumination are shown in figure 1 (b) along with cells with SnO$_2$ only ETL. The average photovoltaic (PV) parameters of the cells at 1 sun: short circuit current (J$_{SC}$), open circuit voltage (V$_{OC}$), fill factor (FF) and power conversion efficiency (PCE) are reported in Table 1. We carried out these tests on 12 different cells for each type obtaining consistent results.

Table 1. Averages of the PV parameters and the maximum PCE of CH$_3$NH$_3$PbI$_3$ planar perovskite solar cells based on SnO$_2$, and Al$_2$O$_3$ spun over the SnO$_2$ surface from the 1.78mg/ml solution at different spin speeds.

D. Characterization

AFM measurements were obtained with peak force tapping imaging technique, employing a Bruker Dimension Icon microscope.

III. RESULTS AND DISCUSSION

The device architecture of the PSCs we fabricated, i.e. ITO/SnO$_2$/Al$_2$O$_3$/CH$_3$NH$_3$PbI$_3$/Spiro-MeOTAD/Au is shown in figure 1 (a). It consisted of a compact SnO$_2$ electron transport layer, known to deliver favorable electron extraction properties, deposited over glass/ITO substrates via low temperature solution processing [28, 34], a CH$_3$NH$_3$PbI$_3$ perovskite semiconductor spin-coated via single-step solvent engineering technique[29], a Spiro-OMeTAD (2,2',7,7'-tetrakis-(N,N-di-p-methoxyphenylamine)-9,9'-spirobifluorene) as hole transport layer, and evaporated Au as top electrode [26]. In particular, we introduced thin Al$_2$O$_3$ nanoparticle interlayers of different thickness between the SnO$_2$ and the perovskite layers by preparing commercially available Al$_2$O$_3$ nanoparticle solution diluted in isopropanol. Three different concentrations (0.59, 0.99 and 1.78mg/ml) of Al$_2$O$_3$ NPs were optimized and 1.78mg/ml was found the best. The Al$_2$O$_3$ solutions were deposited over the SnO$_2$ ETL at different spin speeds (1, 3, 5 and 6 thousand revolutions per
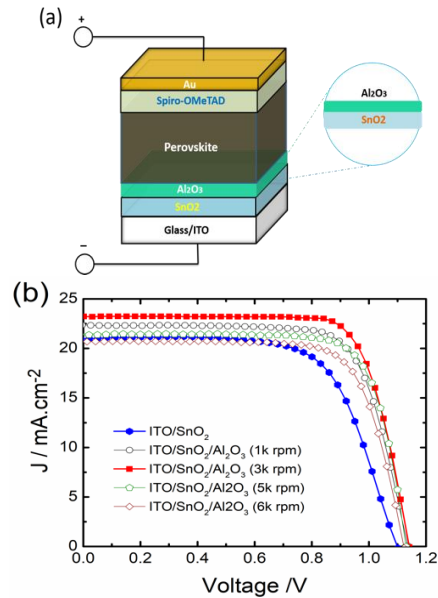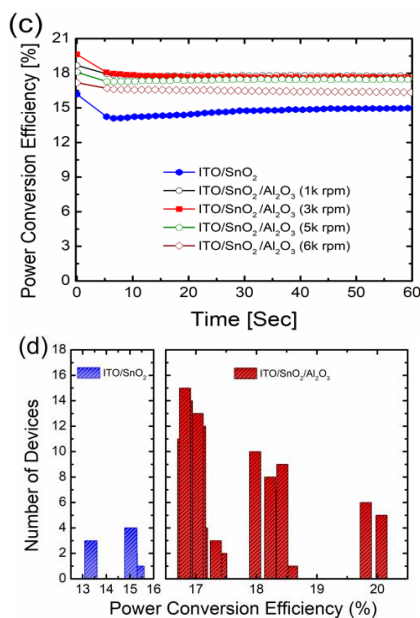
Fig. 1. (a) Device structure of the ITO/SnO$_2$/Al$_2$O$_3$/CH$_3$NH$_3$PbI$_3$/Spiro-MeOTAD/Au perovskite solar cell where Al$_2$O$_3$ (1.78mg/ml) NPs concentration in isopropanol, (b) J-V curves of best performing perovskite solar cell devices based on ITO/SnO$_2$ and ITO/SnO$_2$/Al$_2$O$_3$ bilayers where the Al$_2$O$_3$ was spin coated at different speeds, including 1k rpm, 3k rpm, 5k rpm and 6k rpm under AM1.5G, 1000 W/m^2 irradiation, (c) The evolution of the stabilized power conversion efficiency of the best perovskite solar cells over time measured at constant bias near the maximum power point under AM1.5G, 1000 W/m^2 irradiation. (d) Statistics of PCE distribution for perovskite devices with SnO$_2$ and SnO$_2$/Al$_2$O$_3$ (12 devices).

The PSCs with only SnO$_2$ ETL result in an average PCE of 14.6% (and a maximum PCE of 15.3%) along with a J$_{SC}$ of 20.1 mA/cm^2, V$_{OC}$ of 1.08 V and FF of 66.8%. The PV performance of PSCs was significantly enhanced after introducing the Al$_2$O$_3$ interlayer between the SnO$_2$ and the perovskite films, particularly so at the most favourable concentration (1.78mg/ml) and spin speed (3k rpm). The PCE was measured to be 30% higher in relative terms compared to the SnO$_2$ only counterparts resulting in an average PCE value of 19.1% and a maximum PCE of 20.1% for the best cell.

This increment in PCE is a result of an enhancement in all PV parameters brought about by the incorporation of Al_2O_3. The EQE (external quantum efficiency) was recorded for the best performing device. The integrated Jsc calculated from the EQE with the AM1.5G spectrum was within <10% in relative terms compared to the Jsc measured under 1 sun illumination for cells both with and without Al_2O_3 layer which is well within that expected under these comparisons[36-38].

increased to 17.8% when adding Al_2O_3 deposited at 3 k rpm (at 0.767 V).

The steady state measurements of figure 1c show that the cells have good measurement stability. The statistics of PCE distribution for perovskite devices with SnO_2 and SnO_2/Al_2O_3 was reported in figure 1 (d).

Tapping-mode atomic force microscopy (AFM)

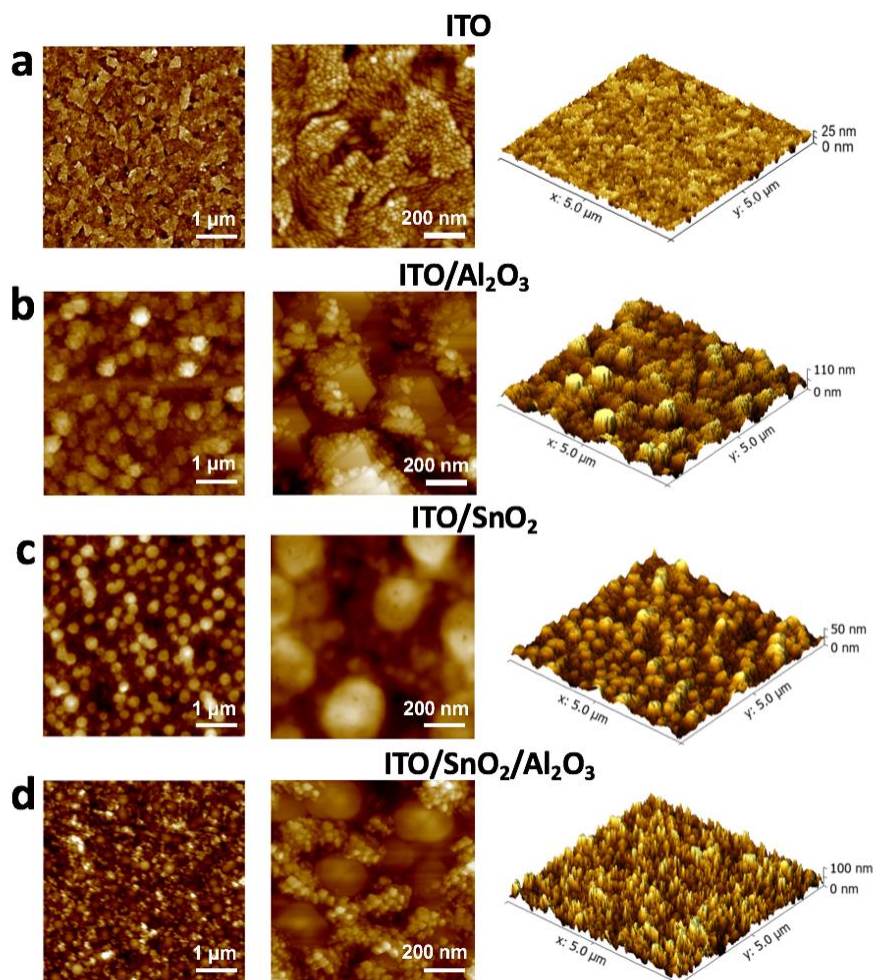**Figure 2.** Atomic Force Microscopy (AFM) images of (a) ITO, (b) ITO/Al₂O₃, (c) ITO/SnO₂ and (d) ITO/SnO₂/Al₂O₃ surface. The scale bar in the first column is 1 μm. The scale bar in the second column is 200nm. The third column shows the 3D images on a 5 μm x 5 μm area where roughness can be gauged.

The photovoltaic parameters for the best cell with the ITO/SnO₂/Al₂O₃ electrode were Jsc = 23.2 mA/cm², FF = 75.7 %, Voc = 1.14V and PCE = 20.1% in reverse scan (and Jsc = 23.4 mA/cm², FF = 71.6%, Voc = 1.10V and PCE = 18.5% in forward scan). The corresponding values for the best cells with ITO/SnO₂ only electrodes were Jsc = 20.5 mA/cm², FF = 68%, Voc = 1.10V and PCE = 15.3% in reverse scan (and Jsc = 20.6 mA/cm², FF = 63%, Voc = 1.08V and PCE = 14.0% in forward scan). Notably, the steady-state efficiencies for all the best devices with different ETLs are reported in Figure 1c versus time (i.e. for 60 seconds) under 1 sun illumination. Measured after 60s, the steady state PCE for the SnO₂–only cell was 14.9% (measured at 0.721V) whereas it

measurements of ITO-only, ITO/Al₂O₃, ITO/SnO₂ and ITO/SnO₂/Al₂O₃ layers were performed to investigate the surface morphology and roughness. Figure 2 (a) shows the surface morphology of the ITO films which were very flat (2.8 nm rms). Addition of the Al₂O₃ on ITO increased the roughness to 25nm and produced a mixed structure of smaller nanoparticles of 15-30nm average dimension and bigger crystallites of the order of 200nm (figure 2b). Differently, the surface roughness of the ITO/SnO₂ was small, i.e. ~9 nm, and showed the presence of round/cylindrical formations of 150-300nm diameter (figure 2c). The smaller sized particles, which can be noted well below the bigger domes, may well be ITO if not smaller sized SnO₂. Finally, the ITO/SnO₂/Al₂O₃ layer in Figure 2d, with a 22nm roughness

(higher than SnO_2 only), resembles in fact the combination of the SnO_2 and the Al_2O_3 films, with larger crystallite/agglomerates (150-200nm) and the smaller nanoparticles. The latter, due to the good visual match with those 15-30nm diameter nanoparticles present in figure 2b can be attributed to Al_2O_3 and may provide a possible explanation of the capability of the Al_2O_3 in reducing defects and filling pinholes in the composite ETL. The higher roughness of the composite SnO_2/Al_2O_3 layer (22nm rms) compared to the SnO_2-only layer (9nm rms) will also determine a different interface when growing the perovskite film as well as a larger electronic interface area.

The dark IV characteristics of best performing PSCs with and without Al_2O_3 interlayer are shown in figure 3 (a). The PSCs with SnO_2/Al_2O_3 double layer delivered a rectification ratio (calculated at +1 V/-1 V) of 1.31×10^3 which was significantly higher compared to that of the cell with only SnO_2 layer (1.89×10^2), showing the higher rectification behavior which is mainly due to a higher forward bias current at 1V. We noticed an increase in fill factor (from 66.1% to 73.1%) for SnO_2/Al_2O_3 measured under 1 sun illumination. In fact, Al_2O_3 over SnO_2 layer provided a better contact resistance between the perovskite and ETL layers [39, 40] as shown in figure 3c.

Al_2O_3 over SnO_2 enhanced the charge transport and electron extraction properties of the PSCs[41]. The OCVR measurements (open circuit voltage rise) under illumination (see figure 3(b)) show that the SnO_2/Al_2O_3 devices delivered a faster rise in Voc compared to the cells with SnO_2 only. This is due to better charge transport from perovskite layer to the charge transport layer and faster extraction. The thin Al_2O_3 layer reduces charge recombination at the interface between perovskite and bottom electrode, leading to enhanced performance. In particular, the series resistance (R_S) and shunt resistance (R_{SH}) of the cells were calculated for both with and without Al_2O_3 (see figure 3(c)). The SnO_2/Al_2O_3 delivered a low R_S ($7.00 \pm 1.1 \ \Omega.cm^2$) value compared to the R_S ($14.72 \pm 2.09 \ \Omega.cm^2$) of cells with SnO_2 only, leading to better charge extraction and passivation of trap states and/or pinholes at the perovskite and SnO_2 interface. Furthermore, R_{SH} calculated for cells with SnO_2/Al_2O_3 layer ($8.27 \pm 1.93 \ k\Omega.cm^2$) is much higher compared to cells with SnO_2 only ($1.4 \pm 0.35 \ k\Omega.cm^2$) which is a result of better interface and/or perovskite film formation over the SnO_2/Al_2O_3 layer and lower recombination[39]. Note that Al_2O_3 is a high band gap insulator[42].
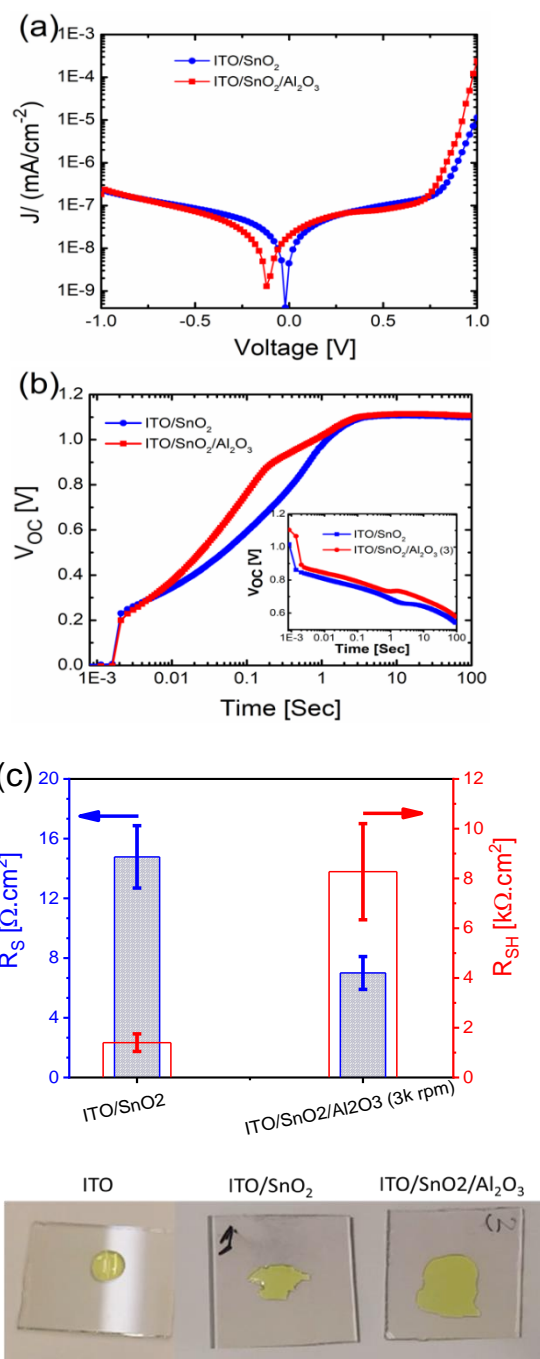
Fig. 3. (a) J-V curves of SnO_2 and SnO_2/Al_2O_3 in dark. Arkeo measurements carried out of perovskite solar cell device using ITO/SnO_2 and $ITO/SnO_2/Al_2O_3$ bilayers under white light irradiation (b) OCVD in light (OCVD in dark inset after switching off the irradiation), and (c) Series resistance (R_S, open squares) and shunt resistance (R_{SH}, closed circles) extracted from the J-V curves of the four cells each under 1 sun irradiation (d) Drop of CH3NH3PbI3 in DMF:DMSO on different ETLs: showing improvement in wettability after Al_2O_3 layer deposition over SnO_2 ETL.

The higher surface roughness of the compact SnO_2/Al_2O_3 bi-compact layer compared to the SnO_2 layer only is likely to be the key reason behind these differences leading to improved interfacial growth of the perovskite and its interface area with the electron-extracting composite electrode [15]. We also

observed that that the presence of UV-irradiated Al_2O_3 enhanced the wettability of SnO_2 layer which determines a larger surface area and better wetting of the precursor (also due to higher surface roughness as discussed in figure 2) as well as network connection and interfacial growth of the perovskite for enhanced charge injection at the interface of perovskite and bottom ETL layer as shown in figure 3 (d) [43, 44].

We also measured the contact potential difference of the ITO/ETL surfaces via Kelvin probe measurements to see whether the application of the metal oxides gave rise to any significant changes in the work function (WF) of the electrodes. With reference to clean ITO electrodes for which WF = 4.70 eV, the WF for ITO/SnO_2 was 4.84 ± 0.12 eV and that of ITO/SnO_2/Al_2O_3 was 4.72 ± 0.05 eV. Thus, the Al_2O_3 overlayer also brings the work function of the electron-extracting electrode 0.1 eV closer to the conduction band of the perovskite solar cell, thereby contributing to the explanation of the higher forward currents at large voltages in the dark. It is very interesting to note that, whereas for the other type of composite bi-layer we had previously developed, i.e. SnO_2/MgO, the insulating MgO overlayer deposited from a precursor solution (rather than from a nanoparticle solution as in this Al_2O_3 case) smoothened the surface and its main effect was to decrease the reverse current in the dark current plots [4] and thus limit back-recombination from the electrode, here the main improvement seen is in forward bias as a result of a lower work function, a more effective charge extraction and better film forming properties as well as maintaining a low reverse current. Thus, the application of thin insulating metal-oxide interlayers over the main transporting compact layers can have two main beneficial different effects apart from suppressing pinholes and trap states (valid for both cases) and/or varying the work function of the electrode which need to be distinguished: a) minimization of charge recombination by enabling electron tunneling from the perovskite to the electrode but suppressing back recombination, or by the small Al_2O_3 nanoparticles more selectively covering those pinhole/defect areas in the underlying compact layer; b) improving perovskite growth and quality of the semiconductor/ETL interface. These effects can even come into play differently when considering the same thin interlayer material, i.e. Al_2O_3, but deposited with different techniques. For example, atomic layer deposition ensures a very thin conformal layer (case a) compared to the rougher surface via solution processed nano-particle thin films here shown (case b) [4, 45-48]and better extracting properties. The enhanced interface area between perovskite and transport layers and improved interfacial growth of the perovskite, as well as reducing the defects/pinholes at the electrode, are likely the major reason for the reduction of charge recombination and improved electron extraction of the perovskite solar cells[15].

IV. CONCLUSION

We have fabricated planar PSCs using SnO_2/Al_2O_3 double ETL between perovskite and ITO bottom electrode. The performance of PSCs was improved significantly after incorporation of SnO_2/Al_2O_3 double ETL. Importantly, SnO_2/Al_2O_3 double ETLs enhanced the PCE of PSCs when measured under 1 sun illumination compared to cells with SnO_2 only. The PSCs with SnO_2/Al_2O_3 double ETL delivered a maximum PCE of 20.1% and a steady state efficiency of 17.8% under 1 sun illumination. These values were 20-30% higher in relative terms compared to that of cells with SnO_2 only (15.3% and 14.9% respectively). We observed that the wettability of SnO_2 layer was effectively enhanced with incorporation of UV-irradiated Al_2O_3 layer. Perovskite solar cells with double ETL delivered higher rectification ratios compared to cells with SnO_2 only. All layers of our device were solution-processed at low temperature ($\leq$ 150 °C). This is a very simple and effective approach for fabricating highly-efficient perovskite cells.

APPENDIX

Appendixes, if needed, appear before the acknowledgement.

REFERENCES

[1] M. A. Green, A. Ho-Baillie, and H. J. Snaith, "The emergence of perovskite solar cells," *Nat Photon,* vol. 8, no. 7, pp. 506-514, 07//print, 2014.

[2] M. G. By Peter K. H. Ho, Richard H. Friend, and Neil C. Greenham, "Ultrathin Self-Assembled Layers at the ITO Interface to Control Charge Injection and Electroluminescence Efficiency in Polymer Light-Emitting Diodes," *Advanced Material,* vol. 10, pp. 1007-0771 1998.

[3] S. D. Stranks, and H. J. Snaith, "Metal-halide perovskites for photovoltaic and light-emitting devices," *Nat Nano,* vol. 10, no. 5, pp. 391-402, 05//print, 2015.

[4] J. Dagar, S. Castro-Hermosa, G. Lucarelli, F. Cacialli, and T. M. Brown, "Highly efficient perovskite solar cells for light harvesting under indoor illumination via solution processed $SnO2$/MgO composite electron transport layers," *Nano Energy,* vol. 49, pp. 290-299, 2018/07/01/, 2018.

[5] D. Yang, R. Yang, K. Wang, C. Wu, X. Zhu, J. Feng, X. Ren, G. Fang, S. Priya, and S. Liu, "High

efficiency planar-type perovskite solar cells with negligible hysteresis using EDTA-complexed SnO2," *Nature Communications,* vol. 9, no. 1, pp. 3239, 2018/08/13, 2018.

[6] M. Dianetti, F. Di Giacomo, G. Polino, C. Ciceroni, A. Liscio, A. D'Epifanio, S. Licoccia, T. M. Brown, A. Di Carlo, and F. Brunetti, "TCO-free flexible organo metal trihalide perovskite planar-heterojunction solar cells," *Solar Energy Materials and Solar Cells,* vol. 140, pp. 150-157, 2015/09/01/, 2015.

[7] Z.-K. Tan, R. S. Moghaddam, M. L. Lai, P. Docampo, R. Higler, F. Deschler, M. Price, A. Sadhanala, L. M. Pazos, D. Credgington, F. Hanusch, T. Bein, H. J. Snaith, and R. H. Friend, "Bright light-emitting diodes based on organometal halide perovskite," *Nat Nano,* vol. 9, no. 9, pp. 687-692, 09//print, 2014.

[8] https://www.nrel.gov/pv/cell-efficiency.html.

[9] A. Kojima, K. Teshima, Y. Shirai, and T. Miyasaka, "Organometal Halide Perovskites as Visible-Light Sensitizers for Photovoltaic Cells," *Journal of the American Chemical Society,* vol. 131, no. 17, pp. 6050-6051, 2009/05/06, 2009.

[10] E. H. Anaraki, A. Kermanpur, L. Steier, K. Domanski, T. Matsui, W. Tress, M. Saliba, A. Abate, M. Grätzel, A. Hagfeldt, and J.-P. Correa-Baena, "Highly efficient and stable planar perovskite solar cells by solution-processed tin oxide," *Energy & Environmental Science,* vol. 9, no. 10, pp. 3128-3134, 2016.

[11] E. Calabrò, F. Matteocci, A. L. Palma, L. Vesce, B. Taheri, L. Carlini, I. Pis, S. Nappini, J. Dagar, C. Battocchio, T. M. Brown, and A. Di Carlo, "Low temperature, solution-processed perovskite solar cells and modules with an aperture area efficiency of 11%," *Solar Energy Materials and Solar Cells,* vol. 185, pp. 136-144, 2018/10/01/, 2018.

[12] C. M. Pelicano, and H. Yanagi, "Efficient solid-state perovskite solar cells based on nanostructured zinc oxide designed by strategic low temperature water oxidation," *Journal of Materials Chemistry C,* vol. 5, no. 32, pp. 8059-8070, 2017.

[13] J. Dagar, G. Scavia, M. Scarselli, S. Destri, M. De Crescenzi, and T. M. Brown, "Coating ZnO nanoparticle films with DNA nanolayers for enhancing the electron extracting properties and performance of polymer solar cells," *Nanoscale,* vol. 9, no. 48, pp. 19031-19038, 2017.

[14] A. Punzi, F. Nicoletta, G. Marzano, C. G. Fortuna, J. Dagar, T. M. Brown, and G. M. Farinola, "Synthetic Routes to TEG-Substituted Diketopyrrolopyrrole-Based Low Band-Gap Polymers," *European Journal of Organic Chemistry,* vol. 2016, no. 19, pp. 3233-3242, 2016.

[15] F. Di Giacomo, V. Zardetto, A. D'Epifanio, S. Pescetelli, F. Matteocci, S. Razza, A. Di Carlo, S. Licoccia, W. M. M. Kessels, M. Creatore, and T. M. Brown, "Flexible Perovskite Photovoltaic Modules and Solar Cells Based on Atomic Layer Deposited Compact Layers and UV-Irradiated TiO2 Scaffolds on Plastic Substrates," vol. 5, no. 8, pp. 1401808, 2015.

[16] T. Gatti, E. Menna, M. Meneghetti, M. Maggini, A. Petrozza, and F. Lamberti, "The Renaissance of fullerenes with perovskite solar cells," *Nano Energy,* vol. 41, pp. 84-100, 2017/11/01/, 2017.

[17] P. Topolovsek, F. Lamberti, T. Gatti, A. Cito, J. M. Ball, E. Menna, C. Gadermaier, and A. Petrozza, "Functionalization of transparent conductive oxide electrode for TiO2-free perovskite solar cells," *Journal of Materials Chemistry A,* vol. 5, no. 23, pp. 11882-11893, 2017.

[18] V. Robbiano, G. M. Paternò, G. F. Cotella, T. Fiore, M. Dianetti, M. Scopelliti, F. Brunetti, B. Pignataro, and F. Cacialli, "Polystyrene nanoparticle-templated hollow titania nanosphere monolayers as ordered scaffolds," *Journal of Materials Chemistry C,* vol. 6, no. 10, pp. 2502-2508, 2018.

[19] F. De Rossi, T. Pontecorvo, and T. M. Brown, "Characterization of photovoltaic devices for indoor light harvesting and customization of flexible dye solar cells to deliver superior efficiency under artificial lighting," *Applied Energy,* vol. 156, pp. 413-422, 2015/10/15/, 2015.

[20] Y. Zhan, Y. Mei, and L. Zheng, "Materials capability and device performance in flexible electronics for the Internet of Things," *Journal of Materials Chemistry C,* vol. 2, no. 7, pp. 1220-1232, 2014.

[21] Y. Chen, Q. Meng, L. Zhang, C. Han, H. Gao, Y. Zhang, and H. Yan, "SnO2-based electron transporting layer materials for perovskite solar cells: A review of recent progress," *Journal of Energy Chemistry,* vol. 35, pp. 144-167, 2019/08/01/, 2019.

[22] C. Wang, L. Guan, D. Zhao, Y. Yu, C. R. Grice, Z. Song, R. A. Awni, J. Chen, J. Wang, X. Zhao, and Y. Yan, "Water Vapor Treatment of Low-Temperature Deposited SnO2 Electron Selective Layers for Efficient Flexible Perovskite Solar Cells," *ACS Energy Letters,* vol. 2, no. 9, pp. 2118-2124, 2017/09/08, 2017.

[23] C. Wang, C. Xiao, Y. Yu, D. Zhao, R. A. Awni, C. R. Grice, K. Ghimire, I. Constantinou, W. Liao, A. J. Cimaroli, P. Liu, J. Chen, N. J. Podraza, C.-S. Jiang, M. M. Al-Jassim, X. Zhao, and Y. Yan, "Understanding and Eliminating Hysteresis for Highly Efficient Planar Perovskite Solar Cells," vol. 7, no. 17, pp. 1700414, 2017.

[24] A. S. Subbiah, N. Mathews, S. Mhaisalkar, and S. K. Sarkar, "Novel Plasma-Assisted Low-Temperature-Processed SnO2 Thin Films for Efficient Flexible Perovskite Photovoltaics," *ACS Energy Letters,* vol. 3, no. 7, pp. 1482-1491, 2018/07/13, 2018.

[25] M. M. Lee, J. Teuscher, T. Miyasaka, T. N. Murakami, and H. J. Snaith, "Efficient Hybrid Solar Cells Based on Meso-Superstructured Organometal Halide Perovskites," *Science,* vol. 338, no. 6107, pp. 643-647, 2012.

[26] J. Dagar, S. Castro-Hermosa, M. Gasbarri, A. L. Palma, L. Cina, F. Matteocci, E. Calabrò, A. Di Carlo, and T. M. J. N. R. Brown, "Efficient fully laser-patterned flexible perovskite modules and solar cells based on low-temperature solution-processed SnO2/mesoporous-TiO2 electron transport layers," vol. 11, no. 5, pp. 2669-2681, May 01, 2018.

[27] A. L. Palma, F. Matteocci, A. Agresti, S. Pescetelli, E. Calabrò, L. Vesce, S. Christiansen, M. Schmidt, and A. D. Carlo, "Laser-Patterning Engineering for Perovskite Solar Modules With 95% Aperture Ratio," *IEEE Journal of Photovoltaics,* vol. 7, no. 6, pp. 1674-1680, 2017.

[28] W. Ke, G. Fang, Q. Liu, L. Xiong, P. Qin, H. Tao, J. Wang, H. Lei, B. Li, J. Wan, G. Yang, and Y. Yan, "Low-Temperature Solution-Processed Tin Oxide as an Alternative Electron Transporting Layer for Efficient Perovskite Solar Cells," *Journal of the American Chemical Society,* vol. 137, no. 21, pp. 6730-6733, 2015/06/03, 2015.

[29] N. Ahn, D.-Y. Son, I.-H. Jang, S. M. Kang, M. Choi, and N.-G. Park, "Highly Reproducible Perovskite Solar Cells with Average Efficiency of 18.3% and Best Efficiency of 19.7% Fabricated via Lewis Base Adduct of Lead(II) Iodide," *Journal of the American Chemical Society,* vol. 137, no. 27, pp. 8696-8699, 2015/07/15, 2015.

[30] A. Agresti, S. Pescetelli, L. Cinà, D. Konios, G. Kakavelakis, E. Kymakis, and A. D. Carlo, "Efficiency and Stability Enhancement in Perovskite Solar Cells by Inserting Lithium-Neutralized Graphene Oxide as Electron Transporting Layer," *Advanced Functional Materials,* vol. 26, no. 16, pp. 2686-2694, 2016.

[31] S. Castro-Hermosa, J. Dagar, A. Marsella, and T. M. Brown, "Perovskite solar cells on paper and the role of substrates and electrodes on performance," *IEEE Electron Device Letters,* vol. 38, no. 9, pp. 1278-1281, 2017.

[32] L. Kegelmann, C. M. Wolff, C. Awino, F. Lang, E. L. Unger, L. Korte, T. Dittrich, D. Neher, B. Rech, and S. Albrecht, "It Takes Two to Tango—Double-Layer Selective Contacts in Perovskite Solar Cells for Improved Device Performance and Reduced Hysteresis," *ACS Applied Materials & Interfaces,* vol. 9, no. 20, pp. 17245-17255, 2017/05/24, 2017.

[33] F. Matteocci, L. Cinà, F. Di Giacomo, S. Razza, A. L. Palma, A. Guidobaldi, A. D'Epifanio, S. Licoccia, T. M. Brown, A. Reale, and A. Di Carlo, "High efficiency photovoltaic module based on mesoscopic organometal halide perovskite," vol. 24, no. 4, pp. 436-445, 2016.

[34] Q. Jiang, L. Zhang, H. Wang, X. Yang, J. Meng, H. Liu, Z. Yin, J. Wu, X. Zhang, and J. You, "Enhanced electron extraction using SnO2 for high-efficiency planar-structure HC(NH2)2PbI3-based perovskite solar cells," *Nature Energy,* vol. 2, pp. 16177, 11/14/online, 2016.

[35] S. Guarnera, A. Abate, W. Zhang, J. M. Foster, G. Richardson, A. Petrozza, and H. J. Snaith, "Improving the Long-Term Stability of Perovskite Solar Cells with a Porous Al2O3 Buffer Layer," *The Journal of Physical Chemistry Letters,* vol. 6, no. 3, pp. 432-437, 2015/02/05, 2015.

[36] H. Xie, X. Yin, J. Liu, Y. Guo, P. Chen, W. Que, G. Wang, and B. Gao, "Low temperature solution-derived TiO2-SnO2 bilayered electron transport layer for high performance perovskite solar cells," *Applied Surface Science,* vol. 464, pp. 700-707, 2019/01/15/, 2019.

[37] J. A. Christians, J. S. Manser, and P. V. Kamat, "Best Practices in Perovskite Solar Cell Efficiency Measurements. Avoiding the Error of Making Bad Cells Look Good," *The Journal of Physical Chemistry Letters,* vol. 6, no. 5, pp. 852-857, 2015/03/05, 2015.

[38] E. Zimmermann, P. Ehrenreich, T. Pfadler, J. A. Dorman, J. Weickert, and L. Schmidt-Mende, "Erroneous efficiency reports harm organic solar cell research," *Nature Photonics,* vol. 8, pp. 669, 09/01/online, 2014.

[39] G.-J. A. H. Wetzelaer, M. Scheepers, A. M. Sempere, C. Momblona, J. Ávila, and H. J. Bolink, "Trap-Assisted Non-Radiative Recombination in Organic–Inorganic Perovskite Solar Cells," *Advanced Materials,* vol. 27, no. 11, pp. 1837-1841, 2015.

[40] A. R. Pascoe, M. Yang, N. Kopidakis, K. Zhu, M. O. Reese, G. Rumbles, M. Fekete, N. W. Duffy, and Y.-B. Cheng, "Planar versus mesoscopic perovskite microstructures: The influence of CH3NH3PbI3 morphology on charge transport and recombination dynamics," *Nano Energy,* vol. 22, pp. 439-452, 2016/04/01/, 2016.

[41] H. Chen, D. Liu, Y. Wang, C. Wang, T. Zhang, P. Zhang, H. Sarvari, Z. Chen, and S. J. N. R. L. Li, "Enhanced Performance of Planar Perovskite Solar Cells Using Low-Temperature Solution-Processed Al-Doped SnO2 as Electron Transport Layers," vol. 12, no. 1, pp. 238, March 31, 2017.

[42] M. Liberatore, L. Burtone, T. M. Brown, A. Reale, A. D. Carlo, F. Decker, S. Caramori, and C. A.

Bignozzi, "On the effect of Al2O3 blocking layer on the performance of dye solar cells with cobalt based electrolytes," *Applied Physics Letters,* vol. 94, no. 17, pp. 173113, 2009.

[43]   A. Fakharuddin, F. Di Giacomo, I. Ahmed, Q. Wali, T. M. Brown, and R. Jose, "Role of morphology and crystallinity of nanorod and planar electron transport layers on the performance and long term durability of perovskite solar cells," *Journal of Power Sources,* vol. 283, pp. 61-67, 2015/06/01/, 2015.

[44]   O. Malinkiewicz, A. Yella, Y. H. Lee, G. M. Espallargas, M. Graetzel, M. K. Nazeeruddin, and H. J. Bolink, "Perovskite solar cells employing organic charge-transport layers," *Nature Photonics,* vol. 8, pp. 128, 12/22/online, 2013.

[45]   H. Si, Q. Liao, Z. Zhang, Y. Li, X. Yang, G. Zhang, Z. Kang, and Y. Zhang, "An innovative design of perovskite solar cells with Al2O3 inserting at ZnO/perovskite interface for improving the performance and stability," *Nano Energy,* vol. 22, pp. 223-231, 2016/04/01/, 2016.

[46]   Y. Wang, T. Mahmoudi, W.-Y. Rho, H.-Y. Yang, S. Seo, K. S. Bhat, R. Ahmad, and Y.-B. Hahn, "Ambient-air-solution-processed efficient and highly stable perovskite solar cells based on CH3NH3PbI3−xClx-NiO composite with Al2O3/NiO interfacial engineering," *Nano Energy,* vol. 40, pp. 408-417, 2017/10/01/, 2017.

[47]   J. Zhang, A. Hultqvist, T. Zhang, L. Jiang, C. Ruan, L. Yang, Y. Cheng, M. Edoff, and E. M. J. Johansson, "Al2O3 Underlayer Prepared by Atomic Layer Deposition for Efficient Perovskite Solar Cells," vol. 10, no. 19, pp. 3810-3817, 2017.

[48]   Y. Du, H. Cai, Z. Xing, Y. Wu, J. Xu, Z. Li, L. Huang, J. Ni, J. Li, and J. Zhang, "Propelling efficiency and stability of planar perovskite solar cells via Al2O3 interface modification to compact TiO2 layer," *Organic Electronics,* vol. 51, pp. 249-256, 2017/12/01/, 2017.